

Giant enhancement of critical current density at high field in superconducting (Li,Fe)OHFeSe films by Mn doping

Dong Li^{1,2}, Jie Yuan^{1,2}, Peipei Shen^{1,2}, Chuanying Xi⁴, Jinpeng Tian^{1,2}, Shunli Ni^{1,2}, Jingsong Zhang^{1,2}, Zhongxu Wei^{1,2}, Wei Hu^{1,2}, Zian Li^{1,2}, Li Yu^{1,3}, Jun Miao⁵, Fang Zhou^{1,2}, Li Pi⁴, Kui jin^{1,2,3}, Xiaoli Dong^{1,2,3, a)}, and Zhongxian Zhao^{1,2,3}

¹Beijing National Laboratory for Condensed Matter Physics, Institute of Physics, Chinese Academy of Sciences, Beijing 100190, China.

²School of Physical Sciences, University of Chinese Academy of Sciences, Beijing 100049, China.

³Songshan Lake Materials Laboratory, Dongguan, Guangdong 523808, China.

⁴Anhui Province Key Laboratory of Condensed Matter Physics at Extreme Conditions, High Magnetic Field Laboratory of the Chinese Academy of Sciences, Hefei 230031, Anhui, China.

⁵Beijing Advanced Innovation Center for Materials Genome Engineering, School of Materials Science and Engineering, University of Science and Technology Beijing, Beijing 100083, China.

^{a)} dong@iphy.ac.cn

Abstract:

Critical current density (J_c) is one of the major limiting factors for high field applications of iron-based superconductors. Here, we report that Mn-ions are successfully incorporated into nontoxic superconducting (Li,Fe)OHFeSe films. Remarkably, the J_c is significantly enhanced from 0.03 to 0.32 MA/cm² under 33 T, and the vortex pinning force density monotonically increases up to 106 GN/m³, which is the highest record so far among all iron-based superconductors. Our results demonstrate that Mn incorporation is an effective method to optimize the performance of (Li,Fe)OHFeSe films, offering a promising candidate for high-field applications.

Introduction

Critical current density, the maximal ability of superconductors to carry current without dissipation, is a crucial factor for high-field applications[1,2]. Among all superconductors, the record J_c value is held so far by the copper oxide superconductors, but their practical application is hampered by a few obstacles[2], such as high anisotropy, a small critical grain boundary angle (θ_c), and a high production cost. On the other hand, iron-based superconductors have moderate anisotropy, a high irreversibility field (H_{irr}), and θ_c , making them more promising for high field application[2-10]. There are still drawbacks for the high-field application of iron-based superconductor. For example, the toxic element arsenic in iron pnictides limits their application although their transition temperature (T_c) and J_c are relatively high[2-5,9]. Therefore, it further research should aim to find nontoxic iron-based superconductors with comparable or even higher J_c .

The nontoxic newly discovered superconductor (Li,Fe)OHFeSe (FeSe-1111)[11], with an optimal T_c of 42 K and a self-field J_c of 0.5 MA/cm² at 20 K under ambient pressure[12], turns out to be a good candidate. However, the vortex pinning potential of FeSe-1111 is relatively low due to the large layer distance[13], leading to the broadening of resistive transition under a magnetic field[14,15]. This calls for further efforts at improving the vortex pinning ability of FeSe-1111, for instance by embedding extra vortex pinning defects[16-19]. Recently, elemental Mn has been incorporated into FeSe-1111 single crystals without obvious detriment to its T_c [20], which may provide an effective candidate. Moreover, iron-based superconductors in the form of films usually present a higher J_c than that of bulk samples[6,8]. Therefore, it is worthy introducing transition metal ions into FeSe-1111 crystalline superconducting film for further optimization of their high-field performance.

In this letter, we successfully introduced Mn-ions into a superconducting FeSe-1111 film synthesized through the so-called

matrix-assisted hydrothermal epitaxy (MHE) method[12]. A significant enhancement of J_c was observed in FeSe-11111 films by Mn-doping, increasing it tenfold from 0.03 to 0.32 MA/cm² under 33 T at 5 K. Remarkably, the vortex pinning force density (F_p) of Mn-doped films monotonically increases to 106 GN/m³. To the best of our knowledge, this is the highest record so far among all iron-based superconducting systems. By analyzing F_p versus magnetic fields, we find the apparent enhancement of J_c in the Mn-doped FeSe-11111 film stems from the extra pinning centers induced by Mn doping.

Experiments

The pure and Mn-doped FeSe-11111 films were synthesized via the MHE method that we developed[12]. The x-ray diffraction (XRD) experiments were carried out on a 9 kW Rigaku SmartLab X-ray diffractometer. The scanning electron microscope (SEM) and energy dispersive X-ray (EDX) spectroscopy measurements were performed on a Hitachi SU5000. The electron energy loss spectroscopy (EELS) data were acquired using a transmission electron microscope (ARM200F, JEOL Inc.) equipped with a Gatan Quantum ER 965 Imaging Filter. Electrical transport measurements within 9T were collected with the standard four-probe method on a Quantum Design PPMS-9 system. The values of J_c were obtained using the criteria of 1 μ V on I-V curves and the parameters of bridge were characterized by SEM. The high-field experiments up to 33 T were performed on the Steady High Magnetic Field Facilities, High Magnetic Field Laboratory, CAS.

Results and discussion

Characterization of crystal structure and elemental Mn

Figure 1(a) shows the XRD patterns of Mn-doped (top) and Mn-free (bottom) FeSe-11111 films, respectively. There are no detectable impurity phases in the Mn-doped system. Moreover, both of them exhibit a single preferred orientation of (001) and the peaks of LaAlO₃ substrates are marked with LAO. The calculated c-axis length decreases from 9.33 Å of the Mn-free film to 9.30 Å of the Mn-doped film, consistent with the result from single crystals[21]. Albeit the full width at half maximum (FWHM) of the rocking curve for the (006) reflection expands from 0.15° to 0.38° due to the presence of Mn-ions, it is still smaller than most of other iron-based superconductor films[22-24], suggesting high crystalline quality. To verify the incorporation of elemental Mn, all the Mn-doped films were checked by EDX spectroscopy or EELS. One of the in-plane SEM images and

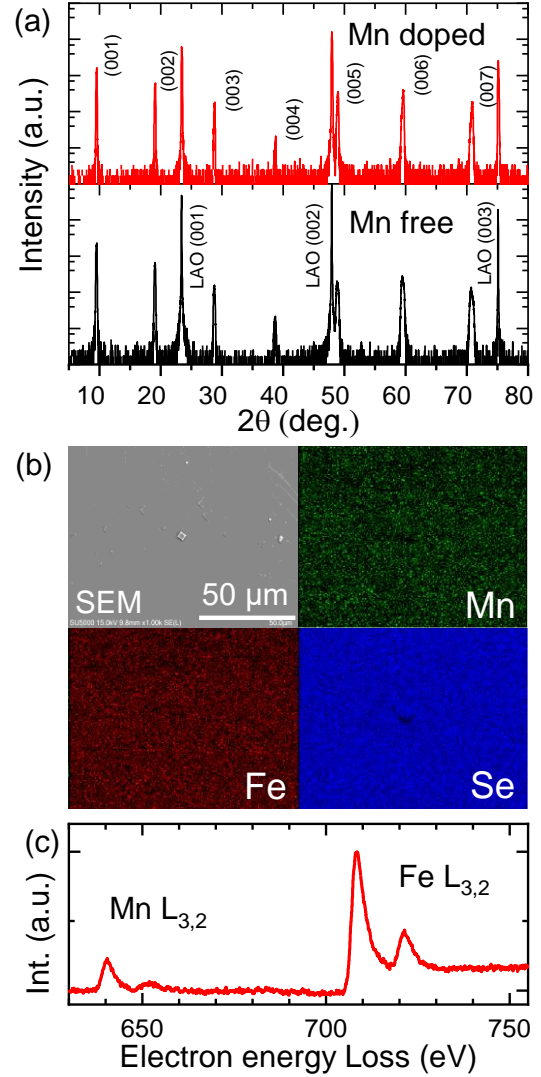


Figure 1. (a) XRD patterns of Mn-doped and Mn-free superconducting FeSe-11111 films, respectively. (b) SEM image and corresponding EDX element mapping of Mn, Fe and Se on the Mn-doped film. (c) The EELS data of Mn-doped FeSe-11111 films.

corresponding EDX mapping of Mn-doped films are shown in Figure 1(b), which display smooth morphology and the uniform distribution of Mn, Fe, and Se elements. The atomic ratio of Mn:Se was determined to be 0.12 by EDX spectroscopy. Moreover, one typical EELS pattern of Mn doped films is shown in Figure 1(c). The presence of L_{3,2} edges for Mn and Fe indicates that Mn ions are incorporated into the lattice of FeSe-11111 films, not left as impurities, which is consistent with the case of Mn-doped FeSe-11111 single crystals[21]. Because of the small difference in ionic sizes for Mn and Fe, it is expected that the incorporated Mn ions substitute for Fe ions at the crystallographic tetrahedral sites. Now that the homogeneous incorporation of Mn-ions has been confirmed in the Mn-doped films, we can make a comparative study on the electrical transport properties between Mn-doped and Mn-free FeSe-11111 films.

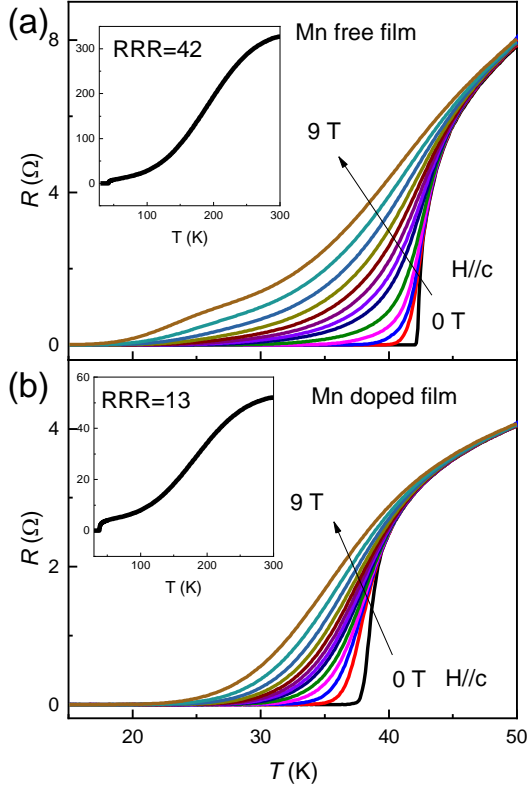


Figure 2. (a) and (b) Temperature dependent resistance of Mn-free and Mn-doped FeSe-11111 films under various *c*-axis magnetic fields up to 9 T, respectively. The insets show the $RRR = R_{300\text{ K}}/R_{50\text{ K}}$ for corresponding films.

The temperature-dependent resistance (R - T) of pure and Mn-doped FeSe-11111 films under *c*-axis magnetic fields are shown in Figures 2(a) and 2(b), respectively. As elemental Mn is incorporated, the T_c , the onset temperature of zero-resistance, declines from 42.0 K to 36.6 K and the residual resistance ratio ($RRR = R_{300\text{ K}}/R_{50\text{ K}}$, insets of Figures 2(a) and 2(b)) decreases from 42 to 13, which indicates that the Mn-ions weakly reduce the superconductivity and serve as extra pairing breaking centers. With increasing fields, the resistive transition becomes broadened and tailed, as widely observed in high- T_c cuprates and iron-based superconductors[25-27], and it is more evident in Mn-free films. This feature is caused by the thermally assisted flux flow and reflects the strength of vortex pinning force[27]. Therefore, the ability of vortex pinning in FeSe-11111 films is indeed improved by Mn doping.

Figure 3(a) displays the representative I - V curves of Mn-doped films, from which the J_c is extracted using the criterion of 1 μV . Figure 3(b) shows the temperature dependence of J_c for Mn-doped (red) and Mn-free (black) films under magnetic fields along (open symbols) or perpendicular (closed symbols) to *c*-axis. The measurable ranges of J_c

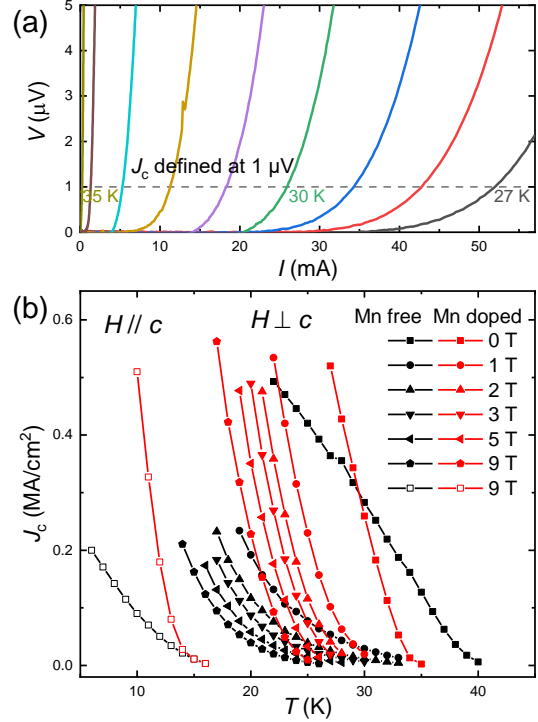


Figure 3. (a) The representative I - V curves of Mn-doped films measured from 35 K to 27 K under 0 T. (b) Temperature dependence of J_c for the Mn-doped (red) and Mn-free (black) films under various applied fields along in-plane ($H \perp c$, closed symbol) and out-of-plane ($H // c$, open symbol), respectively.

were limited by the size of bridges and the upper limit of the applied current, leading to the absence of high J_c data hereafter. Due to the intrinsic electronic two-dimensional (2D) property of FeSe-11111[14], the out-of-plane magnetic field suppresses the superconductivity more prominently than the in-plane one, accounting for the significant J_c anisotropy. It is noted that the J_c values of both Mn-free and Mn-doped films maintain the order of $1 \times 10^5\text{ A/cm}^2$ under 9 T at 10 K, which is higher than the value of $1 \times 10^2\text{ A/cm}^2$ in FeSe-11111 single crystals[28]. The depairing current density of (Li,Fe)OHFeSe can be estimated by $J_0 = \frac{\phi_0}{3\sqrt{3}\mu_0\lambda^2\xi_{ab}}$, where ϕ_0 is the flux quantum, and using values of the penetration depth $\lambda \sim 281\text{ nm}$ [29] and the coherence length $\xi_{ab} \sim 2.21\text{ nm}$ [15]. The calculated value of $J_0 \sim 57.7\text{ MA/cm}^2$ indicates that the FeSe-11111 material has great potential of J_c . Thus, such a dramatic enhancement of J_c is an intrinsic property of the high-quality films [12,30]. It demonstrates that superconducting FeSe-11111 crystalline films are superior to single crystals to achieve high J_c , as commonly seen in other iron-based superconductors[6,8]. Moreover, it is apparent that the enhancement of J_c in FeSe-11111 films by Mn doping under both out-of-plane and in-plane magnetic fields. For instance, the resultant value of J_c increases from 0.9 to $5.1 \times 10^5\text{ A/cm}^2$ under 9 T ($H // c$) at 10 K. Even for the self-field J_c , the performance of Mn-doped

films is superior to Mn-free films below 30 K. In addition, the enhancement of J_c via Mn doping keeps increasing with a decreasing temperature, making the Mn-doped films more interesting in the low-temperature, high-field magnet application. This result confirms that Mn doping is beneficial to the enhancement of J_c for FeSe-1111 films.

Pinning mechanism analysis

To elucidate the origin of J_c enhancement in Mn-doped FeSe-1111 films, we have investigated the magnetic field dependence of F_p ($=J_c \times H$). Due to the strong tail effects of R-T curves, it is difficult to determine the H_{ir} accurately, which is commonly used to normalize the magnetic field[31,32]. In order to improve the accuracy, the normalized pinning force density $f = F_p/F_{p,max}$ is scaled with field $h = H/H_{max}$, where the $F_{p,max}$ is the maximal F_p and H_{max} is the corresponding magnetic field [33,34]. Figure 4 shows plots of scaled data for Mn-doped (red) and Mn-free (black) films. They both follow a temperature independent scaling, indicating there is single dominant pinning mechanism within measured temperature range. Thus, we can analyze the scaling of $f(h)$ by the following equations[18]:

$$f = \frac{9}{4} h \left(1 - \frac{h}{3}\right)^2 \quad \text{for normal point pinning, (1)}$$

$$f = \frac{25}{16} h^{0.5} \left(1 - \frac{h}{5}\right)^2 \quad \text{for normal surface pinning. (2)}$$

It turns out that both cases can be well fitted by equation (2) below H_{max} , demonstrating the dominant pinning mechanism owing to normal surface pinning. These equations actually originate from the Dew-Hughes model[32], where the normal surface pinning refers the pinning centers arising from 2D non-superconducting area such as grain boundaries, plate-like precipitates, and surface of superconductors. This outcome is reasonable given that the insulating (Li,Fe)OH spacer layers may serve as the surface pinning centers in FeSe-1111 superconductors. Meanwhile, above H_{max} , both scaled plots deviate from the theoretical fitting curve, and this deviation is more pronounced in the case of Mn-doped films. The similar feature was also observed in $\text{YBa}_2\text{Cu}_3\text{O}_{7-\delta}$ [33,34], $\text{Bi}_2\text{Sr}_2\text{CaCu}_2\text{O}_{8+x}$ [35], $\text{Nd}_{2-x}\text{Ce}_x\text{CuO}_{4-\delta}$ [36], and Mn doped $\text{K}_x\text{Fe}_{2-y}\text{Se}_2$ single crystals[18], which were attributed to the effect of flux creep. In the normal surface pinning, the F_p is proportional to the pinning center density, implying that the improvement of J_c stems from the extra pinning centers induced by Mn doping. This is consistent with the prior evidence of the expanded FWHM of the rocking curve and the decreased RRR value in Mn-doped films, due to the increase of crystal defects and scattering centers. Further investigation is needed into how the Mn ions affect the vortex behavior of FeSe-1111 films. One possibility we can speculate on is that the Mn ions are doped partly into the (Li,Fe)OH- interlayers, with

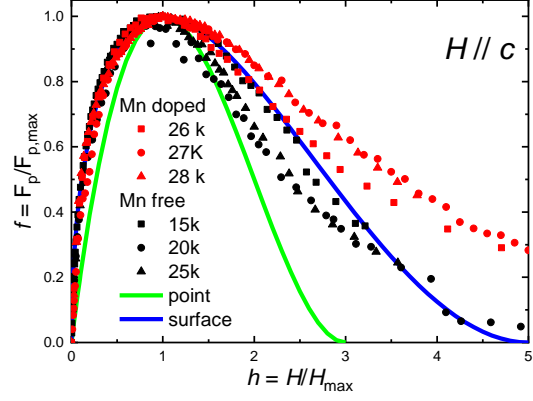


Figure 4. Normalized vortex pinning force density $f = F_p/F_{p,max}$ versus field $h = H/H_{max}$ at various temperature for Mn-doped and Mn-free films. Green line is the fit curve of normal point pinning and the blue line is related to normal surface pinning.

the point defect concentration in the FeSe-layers not sufficient to change the surface pinning behavior.

High-field performance

Figures 5(a) and 5(b) present the data of high-field ($H // c$) J_c and F_p for Mn-doped and pure FeSe-1111 films at 5 K. Data of $\text{SmFeAs}(\text{O},\text{F})$ films[37], $\text{FeSe}_{0.5}\text{Te}_{0.5}$ films[7], P-doped BaFe_2As_2 films[38] and $\text{YBa}_2\text{Cu}_3\text{O}_{7-\delta}$ wires[39] at 4.2 K were also included for comparison. The enhancement of FeSe-1111 films, particularly for the high-field performance, is significant due to Mn doping. Notably, the high field tolerance of J_c for the Mn-doped film overwhelms other iron-based superconductors, which is essential for high-field magnet applications. Numerically, the corresponding J_c increases from 0.03 to 0.32 MA/cm² under 33 T, three times as large as 0.1 MA/cm², the widely accepted value for practical application[2,9]. It is worthy to note that the F_p of the Mn-doped film monotonically increases up to 106 GN/m³, as shown in Figure 5(b), and it is the only iron-based superconductor that resembles the high-field performance of $\text{YBa}_2\text{Cu}_3\text{O}_{7-\delta}$ to date. This feature indicates that the Mn-doped FeSe-1111 films provide a potential extra material for extremely high magnetic field applications, besides cuprates[40]. To our knowledge, the high-field J_c and F_p of Mn-doped FeSe-1111 films obtained in this work set new records so far among all iron-based superconductors. Moreover, the J_c of Mn-doped (Li,Fe)OHFeSe superconductors could be further tuned up to 41 K with proper Mn incorporation[21] and 2) introducing extra artificial pinning centers, similar to proton or ion irradiation, could enhance J_c more significantly[17,19].

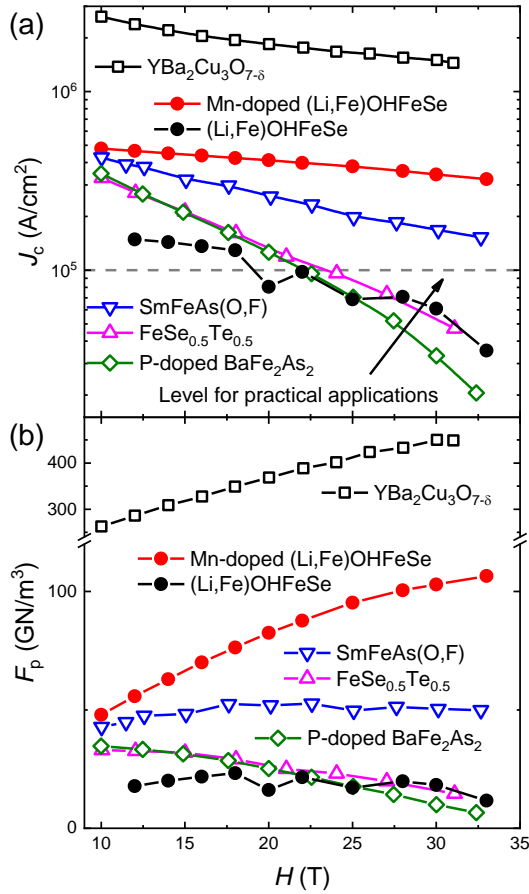


Figure 5. Magnetic field dependence of J_c (a) and F_p (b) of several superconductors, including Mn-doped and pure (Li,Fe)OHFeSe films at 5 K, SmFeAs(O,F) films [37], FeSe_{0.5}Te_{0.5} films [7], P-doped BaFe₂As₂ films [38], and YBa₂Cu₃O_{7-δ} wires [39] at 4.2 K under c-axis fields.

Conclusion

The Mn ions are uniformly incorporated into superconducting FeSe-1111 crystalline films and J_c is remarkably enhanced to 0.32 MA/cm² under 33 T, which is, to our knowledge, the highest reported value so far among various iron-based superconductors. It is found that the normal surface pinning dominates both films and the giant enhancement of J_c stems from extra pinning centers induced by Mn doping. Combined with the energy-saving hydrothermal synthesis, Mn doping method utilized in this work can serve as an easy, fast, and low-cost way to effectively enhance J_c for intercalated iron selenide superconductors. These results demonstrate that the nontoxic Mn-doped superconducting (Li,Fe)OHFeSe crystalline films have very promising prospects of high-field applications.

Acknowledgments

We thank Z. F. Lin and S. S. Yue for valuable discussions. This work was supported by the National Key Research and Development Program of China (Grant Nos. 2017YFA0303003, 2016YFA0300301, 2017YFA0302902, 2018YFB0704102); the National Natural Science Foundation of China (Nos. 11888101, 11834016, 11674374, 11574027); the Strategic Priority Research Program of Chinese Academy of Sciences (XDB25000000), the Strategic Priority Research Program and Key Research Program of Frontier Sciences of the Chinese Academy of Sciences (Grant Nos. QYZDY-SSW-SLH001, QYZDY-SSW-SLH008)

References

- [1] Blatter G., Feigel'man M. V., Geshkenbein V. B., Larkin A. I., and Vinokur V. M. 1994 *Rev. Mod. Phys.* **66** 1125.
- [2] Hosono H., Yamamoto A., Hiramatsu H., and Ma Y. 2018 *Mater. Today* **21** 278
- [3] Hunte F., Jaroszynski J., Gurevich A., Larbalestier D. C., Jin R., Sefat A. S., McGuire M. A., Sales B. C., Christen D. K., and Mandrus D. 2008 *Nature* **453** 903.
- [4] Moll P. J., Puzniak R., Balakirev F., Rogacki K., Karpinski J., Zhigadlo N. D., and Batlogg B. 2010 *Nat. Mater.* **9** 628.
- [5] Katase T., Ishimaru Y., Tsukamoto A., Hiramatsu H., Kamiya T., Tanabe K., and Hosono H. 2011 *Nat. Commun.* **2** 409.
- [6] Li Q., Si W., and Dimitrov I. K. 2011 *Rep. Prog. Phys.* **74** 124510.
- [7] Si W., Han S. J., Shi X., Ehrlich S. N., Jaroszynski J., Goyal A., and Li Q. 2013 *Nat. Commun.* **4** 1347.
- [8] Haindl S., Kiszun M., Oswald S., Hess C., Buchner B., Kolling S., Wilde L., Thersleff T., Yurchenko V. V., Jourdan M., Hiramatsu H., and Hosono H. 2014 *Rep. Prog. Phys.* **77** 046502.
- [9] Zhang X., Yao C., Lin H., Cai Y., Chen Z., Li J., Dong C., Zhang Q., Wang D., Ma Y., Oguro H., Awaji S., and Watanabe K. 2014 *Appl. Phys. Lett.* **104** 202601.
- [10] Hänisch J., Iida K., Hühne R., and Tarantini C. 2019 *Supercond. Sci. Technol.* **32** 093001.
- [11] Lu X. F., Wang N. Z., Wu H., Wu Y. P., Zhao D., Zeng X. Z., Luo X. G., Wu T., Bao W., Zhang G. H., Huang F. Q., Huang Q. Z., and Chen X. H. 2015 *Nat. Mater.* **14** 325.
- [12] Huang Y., Feng Z., Ni S., Li J., Hu W., Liu S., Mao Y., Zhou H., Zhou F., Jin K., Wang H., Yuan J., Dong X., and Zhao Z. 2017 *Chin. Phys. Lett.* **34** 077404.
- [13] Sun Y., Pyon S., Yang R., Qiu X., Feng J., Shi Z., and Tamegai T. 2019 *J. Phys. Soc. Jpn.* **88** 034703.
- [14] Dong X., Jin K., Yuan D., Zhou H., Yuan J., Huang Y., Hua W., Sun J.,

- Zheng P., Hu W., Mao Y., Ma M., Zhang G., Zhou F., and Zhao Z. 2015 *Phys. Rev. B* **92** 064515.
- [15] Wang Z., Yuan J., Wosnitza J., Zhou H., Huang Y., Jin K., Zhou F., Dong X., and Zhao Z. 2017 *J. Phys.: Condens. Matter* **29** 025701.
- [16] Günther A., Deisenhofer J., Kant C., Nidda H. A. K. v., Tsurkan V., and Loidl A. 2011 *Supercond. Sci. Technol.* **24** 045009.
- [17] Fang L., Jia Y., Mishra V., Chaparro C., Vlasko-Vlasov V. K., Koshelev A. E., Welp U., Crabtree G. W., Zhu S., Zhigadlo N. D., Katrych S., Karpinski J., and Kwok W. K. 2013 *Nat. Commun.* **4** 2655.
- [18] Li M., Chen L., You W.-L., Ge J., and Zhang J. 2014 *Appl. Phys. Lett.* **105** 192602.
- [19] Ozaki T., Wu L., Zhang C., Jaroszynski J., Si W., Zhou J., Zhu Y., and Li Q. 2016 *Nat. Commun.* **7** 13036.
- [20] Zhou H., Ni S., Yuan J., Li J., Feng Z., Jiang X., Huang Y., Liu S., Mao Y., Zhou F., Jin K., Dong X., and Zhao Z. 2017 *Chin. Phys. B* **26** 057402.
- [21] Mao Y. Y., Li Z., Zhou H. X., Ma M. W., Chai K., Ni S. L., Liu S. B., Tian J. P., Huang Y. L., Yuan J., Zhou F., Li J. Q., Jin K., Dong X. L., and Zhao Z. X. 2018 *Chin. Phys. B* **27** 077405.
- [22] Iida K., Hänisch J., Hühne R., Kurth F., Kiszun M., Haindl S., Werner J., Schultz L., and Holzapfel B. 2009 *Appl. Phys. Lett.* **95** 192501.
- [23] Takano S., Ueda S., Takeda S., Sugawara H., and Naito M. 2012 *Physica C* **475** 10.
- [24] Feng Z., Yuan J., He G., Hu W., Lin Z., Li D., Jiang X., Huang Y., Ni S., Li J., Zhu B., Dong X., Zhou F., Wang H., Zhao Z., and Jin K. 2018 *Sci. Rep.* **8** 4039.
- [25] Palstra T. T. M., Batlogg B., van Dover R. B., Schneemeyer L. F., and Waszczak J. V. 1990 *Phys. Rev. B* **41** 6621.
- [26] Jia Y., Cheng P., Fang L., Luo H., Yang H., Ren C., Shan L., Gu C., and Wen H.-H. 2008 *Appl. Phys. Lett.* **93** 032503.
- [27] Lee H.-S., Bartkowiak M., Kim J. S., and Lee H.-J. 2010 *Phys. Rev. B* **82** 104523.
- [28] Wang C., Yi X., Qiu Y., Tang Q., Zhang X., Luo Y., and Yu B. 2016 *Supercond. Sci. Technol.* **29** 055003.
- [29] Khasanov R., Zhou H., Amato A., Guguchia Z., Morenzoni E., Dong X., Zhang G., and Zhao Z. 2016 *Phys. Rev. B* **93** 224512.
- [30] Liu Q., Chen C., Zhang T., Peng R., Yan Y.-J., Wen C.-H.-P., Lou X., Huang Y.-L., Tian J.-P., Dong X.-L., Wang G.-W., Bao W.-C., Wang Q.-H., Yin Z.-P., Zhao Z.-X., and Feng D.-L. 2018 *Phys. Rev. X* **8** 041056.
- [31] Kramer E. J. 1973 *J. Appl. Phys.* **44** 1360.
- [32] Dew-Hughes D. 1974 *Philos. Mag.* **30** 293.
- [33] Civalè L., McElfresh M. W., Marwick A. D., Holtzberg F., Feild C., Thompson J. R., and Christen D. K. 1991 *Phys. Rev. B* **43** 13732.
- [34] Higuchi T., Yoo S. I., and Murakami M. 1999 *Phys. Rev. B* **59** 1514.
- [35] Prischepa S. L., Attanasio C., Coccoresse C., Maritato L., Pourtier F., Salvato M., and Kushnir V. N. 1996 *J. Appl. Phys.* **79** 4228.
- [36] Cirillo C., Guarino A., Nigro A., and Attanasio C. 2009 *Phys. Rev. B* **79** 144524.
- [37] Iida K., Hänisch J., Tarantini C., Kurth F., Jaroszynski J., Ueda S., Naito M., Ichinose A., Tsukada I., Reich E., Grinenko V., Schultz L., and Holzapfel B. 2013 *Sci. Rep.* **3** 2139.
- [38] Kurth F., Tarantini C., Grinenko V., Hänisch J., Jaroszynski J., Reich E., Mori Y., Sakagami A., Kawaguchi T., Engelmann J., Schultz L., Holzapfel B., Ikuta H., Hühne R., and Iida K. 2015 *Appl. Phys. Lett.* **106** 072602.
- [39] Xu A., Jaroszynski J. J., Kametani F., Chen Z., Larbalestier D. C., Viouchkov Y. L., Chen Y., Xie Y., and Selvamanickam V. 2010 *Supercond. Sci. Technol.* **23** 014003.
- [40] Hahn S., Kim K., Kim K., Hu X., Painter T., Dixon I., Kim S., Bhattarai K. R., Noguchi S., Jaroszynski J., and Larbalestier D. C. 2019 *Nature* **570** 496.